INDIAN JOURNAL OF SCIENCE AND TECHNOLOGY

RESEARCH ARTICLE

Check for updates

OPEN ACCESS

**Received:** 15-07-2024

**Accepted:** 21-08-2024

**Published:** 12-09-2024

**Citation:** Lamzamuan G, Devi SK, Gogoi L (2024) Unraveling the Protolith Origin of Serpentinite Rocks from the Tengnoupal Area, Manipur Ophiolite Complex, Indo-Myanmar Range. Indian Journal of Science and Technology 17(36): 3719-3732. https://doi.org/10.17485/IJST/v17i36.2279

* **Corresponding author**.

sorokhaibamkavita@gmail.com

**Funding:** CSIR-NET(JRF)

**Competing Interests:** None



Published By Indian Society for Education and Environment (iSee)

**ISSN**
Print: 0974-6846
Electronic: 0974-5645

# Unraveling the Protolith Origin of Serpentinite Rocks from the Tengnoupal Area, Manipur Ophiolite Complex, Indo-Myanmar Range

**G Lamzamuan[1], Sorokhaibam Kavita Devi[2]*, Liza Gogoi[1]**

**1** Research Scholar, Department of Geology, Mizoram University, Aizawl, Mizoram, India
**2** Assistant professor, Department of Geology, Mizoram University, Aizawl, Mizoram, India

## Abstract

**Objective:** This article mainly focuses on investigating the protolith origin of serpentinite rocks in and around Tengnoupal, within the Manipur Ophiolite Complex (MOC), using a combined petrographic and geochemical approach. **Methods:** During fieldwork, samples were collected and cut into thin sections to reveal their mineralogical and textural relationships. Major oxides and trace elements were determined by XRF, and rare earth elements analysis was carried out by ICP-MS to determine the nature and origin of the rocks. **Findings:** The studied rock samples exhibit varying degrees of serpentinization, ranging from partial to complete, and exhibit a pseudomorphic texture including mesh and hour structures replacing the original olivine and bastite texture replacing pyroxene. Geochemically, the analyzed rock types exhibit komatiitic affinity and are characterized by high magnesium numbers (Mg# average 84.4). The studied serpentinite rocks have lower Al/Si ratios (Average=0.05) and higher Mg/Si ratios (average= 0.95) in bulk rock compositions indicating a refractory abyssal mantle peridotite protolith when compared to the primitive mantle. The high Ti (range 300-480 ppm) and Cr (628-3186 ppm) contents indicate a subduction environment. In addition, the rock samples exhibit slight depletion chondrite-normalized Rare Earth Elements (REE) patterns ($(La/Yb)_N$ = average 0.87). The rocks exhibit spoon-shaped normalized Rare Earth Element patterns and primitive mantle are similar to mid-oceanic ridge abyssal mantle rocks. **Novelty:** The origins of the rocks studied suggest a transitional phase between abyssal and subduction zone-related serpentinites, forming after harzburgite-peridotite. As subduction began, dehydrated orogenic peridotite from the abyssal serpentinites was thrust or obducted, forming the MOC serpentinites. This indicates that the serpentinite rocks in MOC share similarities with those found in mid-oceanic ridge environments, which is characteristic of a supra-subduction zone setting.

**Keywords:** Ultramafic rocks; Serpentinization; Suprasubduction zone; Abyssal; REE

# 1 Introduction

Ophiolite-related ultramafic rocks are found along the Indo-Myanmar range within the Manipur Ophiolite Complex. These ultramafic rocks formed in the Earth's upper mantle and subsequently transformed into serpentinites, either completely or partially, through the interaction with crustal fluids during their movement to their current tectonic location. Ophiolites provide valuable insights into the evolution of ancient oceanic crust and mantle beneath spreading centers, including Mid-Ocean Ridge (MOR) and Supra-Subduction Zone (SSZ) tectonic settings[(1,2)]. They form in diverse tectonic environments, both related and unrelated to subduction processes[(3)]. From the study of the geochemical composition of ophiolitic rocks various tectonic environments such as sea-floor spreading zones, hotspots, backarc and forearc basins (SSZ environments), and other extensional magmatic tectonic settings, including those associated with plumes can be identified and understand the nature of mantle sources. In addition, ophiolites also provide information about the metamorphic, magmatic, and tectonic processes of the oceanic crust and upper mantle[(4)]. Ophiolitic mantle rocks are primarily important for understanding the palaeotectonic development of the oceanic lithosphere, partial melting, melt-rock interaction, and mantle melt fractionation[(4)]. In particular, abyssal peridotites are remnants of partially melted mantle below MOR, while highly depleted SSZ-type peridotites are mantle rocks that have undergone intense melting above subduction zones[(2)].

The MOC consists of well-preserved mantle peridotite and chromite with a minor amount of mafic and felsic rocks along with Oceanic Pelagic Sediments (OPS). The mantle peridotite consists predominantly of harzburgite and lherzolite[(5)]. Serpentinized peridotite is the major component of the MOC while intrusive and extrusive mafic rocks form the minor components. The residual ultramafic rocks of lherzolite and harzburgite in the MOC are derivatives of spinel lherzolite that have undergone varying degrees of partial melting[(6)]. The MOC shows wide variation in its geochemical composition.

Several workers have studied the Naga-Manipur Ophiolite Belt (NMOB) in various aspects such as the NMOB consists of tectonic peridotite, mafic-ultramafic cumulate, mafic volcanic and dykes, plagiogranite, and OPS[(1,7)]. It was reported to have formed in the SSZ, possibly during forearc-back arc magmatism when the India plate was subducting beneath the Myanmar plate[(2,7,8)]. The ophiolite formed in the spreading center of MOR or Plume-type features[(9,10)]. The serpentinites are the predominant rock type in the MOC area and have been largely neglected. In this present investigation, the main emphasis is given to the petrology and geochemical aspects like petrography, major, trace, and Rare Earth Elements (REE) of the area to understand and also correlate the protolith and geotectonic setting of these serpentinite rocks and characterize the nature of NMOB exposures in larger extent.

## 1.1 Geological Setting

The NMOB within the Alpine-Himalayan orogenic system forms a prominent NNE-SSW trending arcuate belt along the Indo-Myanmar Range (IMR). This belt is a part of the Arakan Yoma-Chin Hills-Naga Hills flysch trough, which dates back to the Upper Cretaceous to the Middle Eocene. This ophiolite appears as irregular tectonic blocks along the eastern margin of the IMR and extends up to the Andaman-Nicobar Islands. The NMOB is interpreted as an accretionary prism formed by the convergence of the Indian plate with the Myanmar plate[(11)]. The ophiolitic rocks within the Indo-Myanmar Orogenic Belt (IMOB) show extensive tectonic deformation and fragmentation, reflecting three distinct phases of geological events similar to both the Himalayan orogeny and seafloor spreading observed in the Indian Ocean. These dismembered basic and ultrabasic rocks are closely associated with oceanic pelagic sediments and occur as folded thrust slices that overlay distal shelf sedimentary rocks ranging from the Eocene to Oligocene periods[(9)].

The MOC thrusts over the Disang turbidites on the west, while the east of the state is covered by a very limited exposure of metamorphic rocks. These pre-Mesozoic metamorphic rocks, consisting of low to medium-grade phyllitic schist, quartzite, marble, and granite-gneiss, are considered the oldest unit in this region[(6,9)]. The ultramafic serpentinites represent the largest litho-unit, making up more than 90% of the igneous ophiolitic exposures with oceanic pelagic sediment and various blocks of exotic rocks. These exotic blocks are mainly Oceanic pelagic Shale-hosted while some of them especially gritty sandstones are found on Ultramafic rocks. The exposures of mafic rocks, including extrusive pillow lavas and diabasic dyke rocks which are sandwiched within the pelagic shale were also observed in the complex[(6)]. The ophiolite complex is placed within the Disang Group of the Eocene to Upper Cretaceous age. The study area lies in the southeastern sector of the Tengnoupal district within Manipur state, as illustrated (Figure 1**a** and **b**). The ultramafic rock suite in this region predominantly comprises mantle peridotites, which are closely related to pelagic sediments such as chert, conglomerates, slates, and shales. The residual mantle peridotite mainly consists of metamorphosed harzburgite and lherzolite, while the remaining 10% is made up of basic dykes and sills and volcanic rocks, including pillow lavas[(6)]. The petrogenetic and structural characteristics of the NMOB reflect the evolution of the Tethyan oceanic crust and upper mantle. This development occurred in a changing geodynamic environment characterized by SSZ forearc extension, subduction initiation, and continental arc accretion[(1)]. The ultramafic serpentinized peridotites of a Neo-Tethyan mantle wedge underwent varying degrees of mantle metasomatism and partial melting[8]. The belt is thought to have formed in a complex tectonic setting involving MOR and subduction zone processes[12].

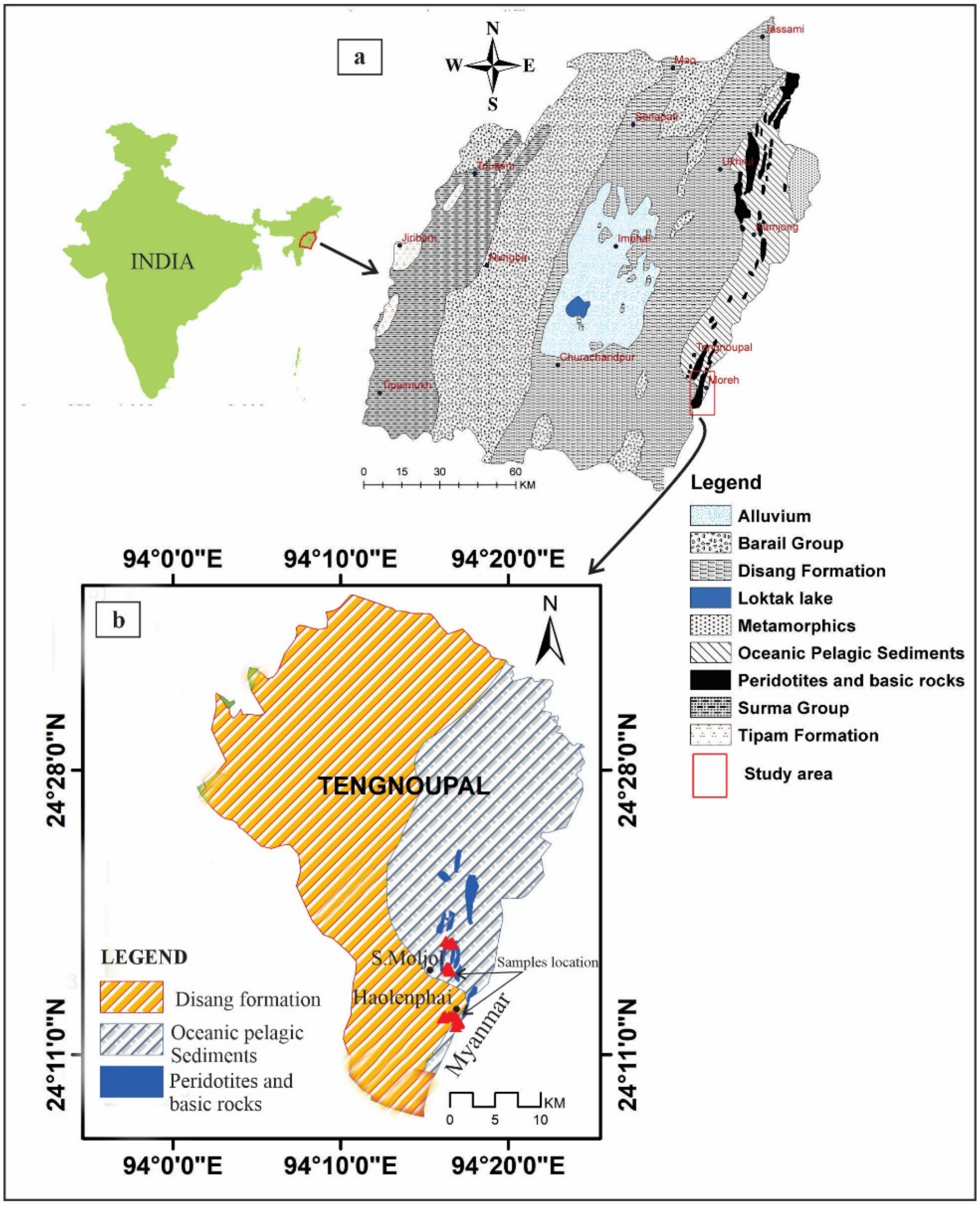


**Fig 1. a) Generalized geological map of Manipur Northeast India and b) Geological map of the study area in MOC of Tengnoupal**

## 2 Methodology

In this study, detailed fieldwork was carried out in which 30 representative rock samples were collected from the study area (Figure 1**b**). These samples were sent to the Department of Geological Sciences, Gauhati University, Guwahati for slide preparation. Out of these, 10 samples were selected for geochemical analyses for this work. Petrographic analyses were carried out using a Leica DME2700P petrological microscope equipped with a Leica DFC420 camera and Leica Image analysis software (LAS-V.4.6) at the Department of Geology, Mizoram University.

Whole-rock analysis for major, trace, and rare earth elements (REE) was carried out at the Wadia Institute of Himalayan Geology in Dehradun, India. Major oxides and trace elements were determined using an X-ray Fluorescence spectrometer (XRF) on a Bruker S8 Tiger. The sample preparation involved drying powdered samples (200 mesh) at 105°C for 12 hours followed by high-temperature ashing at 1,000°C for 5 hours. The resulting materials were then cooled (400°C), and reweighed to determine the Loss on Ignition (LOI). The analytical precision was within ± 2% to 3% for major elements and ± 5% to 6% for trace elements. Rare earth elements were analyzed using a Quadrupole Inductively Coupled Plasma Mass Spectrometer (TQ-ICP-MS; Perkin Elmer SCIEX ELAN DRC-II). The comprehensive geochemical data are shown in Table 1.

**Table 1. Whole-rock of Major, trace, and rare earth elements of Serpentinite rocks in MOC**

| Sample | HZ25 | HZ26 | HZ27 | HP8 | HP9 | HP12 | HP13 | HP14 | HP16 | HP18 |
|---|---|---|---|---|---|---|---|---|---|---|
| **Major oxide elements (wt.%)** | | | | | | | | | | |
| $SiO_2$ | 41.29 | 41.06 | 42.02 | 41.03 | 39.94 | 41.28 | 40.11 | 40.73 | 40.32 | 41.60 |
| $Al_2O_3$ | 2.40 | 2.29 | 3.01 | 2.27 | 2.27 | 2.50 | 2.07 | 2.34 | 2.78 | 0.95 |
| $Fe_2O_3$ | 6.35 | 5.71 | 8.03 | 7.22 | 7.50 | 7.93 | 8.24 | 7.82 | 7.34 | 5.11 |
| CaO | 0.99 | 0.58 | 1.61 | 1.06 | 0.77 | 1.72 | 0.41 | 0.69 | 1.79 | 0.02 |
| MgO | 38.50 | 39.60 | 36.13 | 38.90 | 39.28 | 37.84 | 40.07 | 38.21 | 38.69 | 42.60 |
| $K_2O$ | 0.02 | 0.00 | 0.00 | 0.00 | 0.00 | 0.00 | 0.00 | 0.00 | 0.00 | 0.00 |
| $Na_2O$ | 0.05 | 0.05 | 0.06 | 0.06 | 0.05 | 0.06 | 0.05 | 0.05 | 0.05 | 0.04 |
| MnO | 0.10 | 0.11 | 0.11 | 0.11 | 0.13 | 0.11 | 0.09 | 0.11 | 0.08 | 0.07 |
| $TiO_2$ | 0.07 | 0.06 | 0.08 | 0.07 | 0.07 | 0.08 | 0.05 | 0.05 | 0.07 | 0.00 |
| $P_2O_5$ | 0.00 | 0.01 | 0.00 | 0.00 | 0.00 | 0.00 | 0.00 | 0.00 | 0.00 | 0.00 |
| Total | 89.77 | 89.47 | 91.05 | 90.72 | 90.01 | 91.52 | 91.09 | 90.00 | 91.12 | 90.39 |
| LOI | 14.09 | 14.04 | 13.89 | 12.45 | 13.43 | 13.20 | 12.22 | 14.37 | 12.81 | 13.44 |
| Mg# | 87 | 88 | 83 | 86 | 85 | 72 | 84 | 84 | 85 | 90 |
| MgO/SiO2 | 0.93 | 0.96 | 0.86 | 0.95 | 0.98 | 0.92 | 0.99 | 0.94 | 0.96 | 1.02 |
| $Al_2O_3/SiO_2$ | 0.05 | 0.05 | 0.07 | 0.05 | 0.06 | 0.06 | 0.05 | 0.06 | 0.07 | 0.02 |
| **Trace elements (ppm)** | | | | | | | | | | |
| Ba | - | - | 9 | - | - | - | - | 16 | 9 | 13 |
| Cr | 3816 | 3516 | 3489 | 3188 | 2817 | 3189 | 2916 | 2987 | 2839 | 628 |
| V | 74 | 62 | 89 | 78 | 74 | 90 | 77 | 67 | 78 | 6 |
| Sc | 14 | 13 | 11 | 12 | 14 | 13 | 13 | 9 | 10 | - |
| Co | 126 | 124 | 31 | 114 | 99 | 108 | 114 | 71 | 54 | 114 |
| Ni | 2347 | 2710 | 4074 | 2269 | 2264 | 2369 | 2265 | 3331 | 3236 | 2921 |
| Cu | 36 | 14 | 26 | 23 | 20 | 22 | 21 | 19 | 6 | 32 |
| Zn | 53 | 55 | 47 | 64 | 47 | 58 | 48 | 49 | 30 | 38 |
| Ga | - | - | - | - | - | - | - | - | - | - |
| Pb | - | - | - | - | - | - | - | - | - | - |
| Th | - | 2.1 | - | 1.3 | 1.8 | 2.1 | - | 0.1 | 1.4 | 1.5 |
| Rb | - | - | - | - | - | - | - | - | - | - |
| U | 0.5 | 0.6 | 0.3 | 0.4 | 0.4 | 0.3 | 0.4 | 0.4 | 0.4 | 0.7 |
| Sr | - | - | - | 1 | 6 | 1 | 2 | 1 | - | - |
| Y | 4 | 3 | 4 | 4 | 4 | 4 | 4 | 4 | 6 | 3 |
| Zr | - | 3 | 3 | - | - | - | - | - | - | - |
| Nb | - | - | - | - | - | - | - | - | - | - |
| **Rare earth elements (ppm)** | | | | | | | | | | |
| La | 0.022 | 0.022 | 0.062 | 0.074 | 0.010 | 0.030 | 0.002 | 0.346 | 1.778 | 0.032 |
| Ce | 0.108 | 0.078 | 0.036 | 0.200 | 0.056 | 0.074 | 0.020 | 0.112 | 0.248 | 0.098 |
| Pr | 0.014 | 0.012 | 0.010 | 0.018 | 0.006 | 0.008 | 0.000 | 0.016 | 0.270 | 0.004 |
| Nd | 0.086 | 0.070 | 0.046 | 0.092 | 0.056 | 0.056 | 0.008 | 0.060 | 0.536 | 0.028 |
| Sm | 0.104 | 0.068 | 0.046 | 0.064 | 0.060 | 0.084 | 0.014 | 0.050 | 0.222 | 0.006 |
| Eu | 0.040 | 0.024 | 0.022 | 0.028 | 0.032 | 0.034 | 0.006 | 0.022 | 0.068 | 0.010 |
| Gd | 0.182 | 0.120 | 0.100 | 0.128 | 0.138 | 0.168 | 0.034 | 0.108 | 0.352 | 0.006 |
| Tb | 0.040 | 0.026 | 0.022 | 0.026 | 0.030 | 0.038 | 0.008 | 0.022 | 0.058 | 0.000 |
| Dy | 0.310 | 0.202 | 0.166 | 0.220 | 0.244 | 0.310 | 0.074 | 0.192 | 0.420 | 0.006 |
| Ho | 0.076 | 0.048 | 0.040 | 0.052 | 0.060 | 0.076 | 0.018 | 0.048 | 0.104 | 0.002 |
| Er | 0.224 | 0.140 | 0.128 | 0.162 | 0.176 | 0.222 | 0.060 | 0.140 | 0.298 | 0.006 |

*Continued on next page*

*Table 1 continued*

| | | | | | | | | | | |
|---|---|---|---|---|---|---|---|---|---|---|
| Tm | 0.038 | 0.022 | 0.020 | 0.026 | 0.030 | 0.038 | 0.010 | 0.022 | 0.046 | 0.002 |
| Yb | 0.236 | 0.166 | 0.124 | 0.198 | 0.204 | 0.256 | 0.064 | 0.172 | 0.284 | 0.010 |
| Lu | 0.038 | 0.026 | 0.020 | 0.030 | 0.032 | 0.042 | 0.010 | 0.028 | 0.048 | 0.002 |
| ΣREE | 1.518 | 1.024 | 0.842 | 1.318 | 1.134 | 1.436 | 0.328 | 1.338 | 4.732 | 0.212 |
| ΣLREE | 0.374 | 0.274 | 0.222 | 0.476 | 0.220 | 0.286 | 0.050 | 0.606 | 3.122 | 0.178 |
| ΣHREE | 1.144 | 0.750 | 0.620 | 0.842 | 0.914 | 1.150 | 0.278 | 0.732 | 1.610 | 0.034 |
| (La/Yb)N | 0.063 | 0.090 | 0.339 | 0.254 | 0.033 | 0.079 | 0.021 | 1.366 | 4.253 | 2.174 |
| (Gd/Yb)N | 0.624 | 0.585 | 0.652 | 0.523 | 0.547 | 0.530 | 0.429 | 0.508 | 1.003 | 0.485 |
| (Ce/Sm)N | 0.257 | 0.284 | 0.194 | 0.775 | 0.231 | 0.218 | 0.354 | 0.555 | 0.277 | 4.050 |
| Eu/Eu* | 0.857 | 0.783 | 0.956 | 0.912 | 1.037 | 0.844 | 0.810 | 0.882 | 0.717 | 4.912 |
| Ce/Ce* | 1.482 | 1.156 | 0.348 | 1.320 | 1.741 | 1.151 | 3.551 | 0.362 | 0.086 | 2.086 |

LOI: Loss on Ignition; Mg#: Magnesium number and -: Below detection limit.

## 3 Results and Discussion

### 3.1 Petrography:

The serpentinite rocks of the MOC found in Haolenphai and New Mongjang villages of the Tengnoupal area, are mainly composed of olivine and pyroxene and exhibit varying degrees of serpentinization. According to the thin section, pseudomorphic textures such as mesh and hourglass textures after olivine and bastites after pyroxene minerals (orthopyroxene) as well as fibrous structures, filling the veins by chrysotile are observed (Figure 2**a, b, c & d**). The presence of abundant bastite suggests that the original rock, or protolith, was likely harzburgite. Olivines are anhedral to subhedral and range from 0.3 to 0.5 mm in diameter and highly fractured and these grains display hourglass texture indicating significant metamorphic processes. Orthopyroxene appears as pale brownish, subhedral grains, often forming large porphyroclasts up to a centimeter in size. Many orthopyroxene porphyroclasts have experienced significant deformation, undulatory extinction, and kink banding providing evidence of strain effect (Figure 2**e**). Also, in some bastite sections, rare exsolution lamellae of clinopyroxene (Cpx) are also preserved and talc or chlorite alteration primarily occurring along the cleavage planes (Figure 2**f**), and exhibit lobate grain boundaries. Opaque minerals like chromium-spinel and magnetite are also observed, and the cr-spinel grains are more abundant than the magnetite. They are characterized by their brown to reddish-brown color often found along olivine fractures and also occur between pyroxene and serpentinite indicating formation before serpentinization (Figure 2 **g**). It also has an opaque Fe-rich that resembles magnetite rims. In addition, secondary magnetite minerals have formed along grain boundaries and fractures due to the weathering of mafic minerals.

### 3.2 Major oxide elements:

Bulk rock major elements of ten chosen samples of the serpentinite rocks from the MOC are given in Table 1. The analyzed sample's Loss on Ignition (LOI) ranges from 12.22 to 14.37 wt.%. These relatively high LOI values indicate significant serpentinization of olivine and pyroxene, as supported by petrographic analysis. The low $SiO_2$ content of the samples ranges from 39.94 to 41.60 wt.%. The majority of the samples contain high MgO ranging from 36.13 to 42.60 wt.%; low $Al_2O_3$ values ranging from 0.95 to 3.01 wt.% and the magnesium number (Mg#) between 72-90 wt.%. The major elements of the studied ultramafic rocks in MOC align with metamorphic peridotites on the ACM ($Al_2O_3$-CaO- MgO) and AFM [($Na_2O$-$K_2O$)-FeO-MgO)] of the ternary diagram (Figure 3 **a** and **b**)[(13)]. This suggests that the serpentinites examined represent a depleted or residual mantle. These results are further supported by high Mg# values. In particular, Mg# values of some of the samples examined are 84.40, which is close to the primitive mantle value of 89 (Sun and Mc Donough 1989) and comparable to the Mg# values found in residual peridotites. According to [($FeO_t$+$TiO_2$)–$Al_2O_3$-MgO], the ternary diagram illustrates the komatiitic affinity of serpentinite rocks[(14)] (Figure 3 **c**).

The rocks studied have a higher Mg/Si ratio (ranging from 0.85 to 1.02 with an average value of 0.89) compared to the primitive mantle value (0.85), but a lower Al/Si ratio (ranging from 0.023 to 0.072 with an average value of 0.040) than the primitive mantle PM value 0.1 (Sun and Mc Donough 1989). The Al/Si ratios in the serpentinite rocks were often lower than the PM value of 0.1 (Sun and Mc Donough 1989) but greater than the highly depleted mantle residual harzburgites, which had an Al/Si ratio of approximately 0.02. The lower $Al_2O_3/SiO_2$ ratios in the serpentinite peridotites relative to the PM values suggest that the protoliths partially melted before serpentinization[(15)]. The variation diagram of major oxide elements (Figure 4), where $Al_2O_3$ was utilized as a depletion index among the least mobile elements to understand better specific elements' behavior[(15)]. Major oxide elements like MgO have a negative correlation and $Na_2O$ does not correlate with

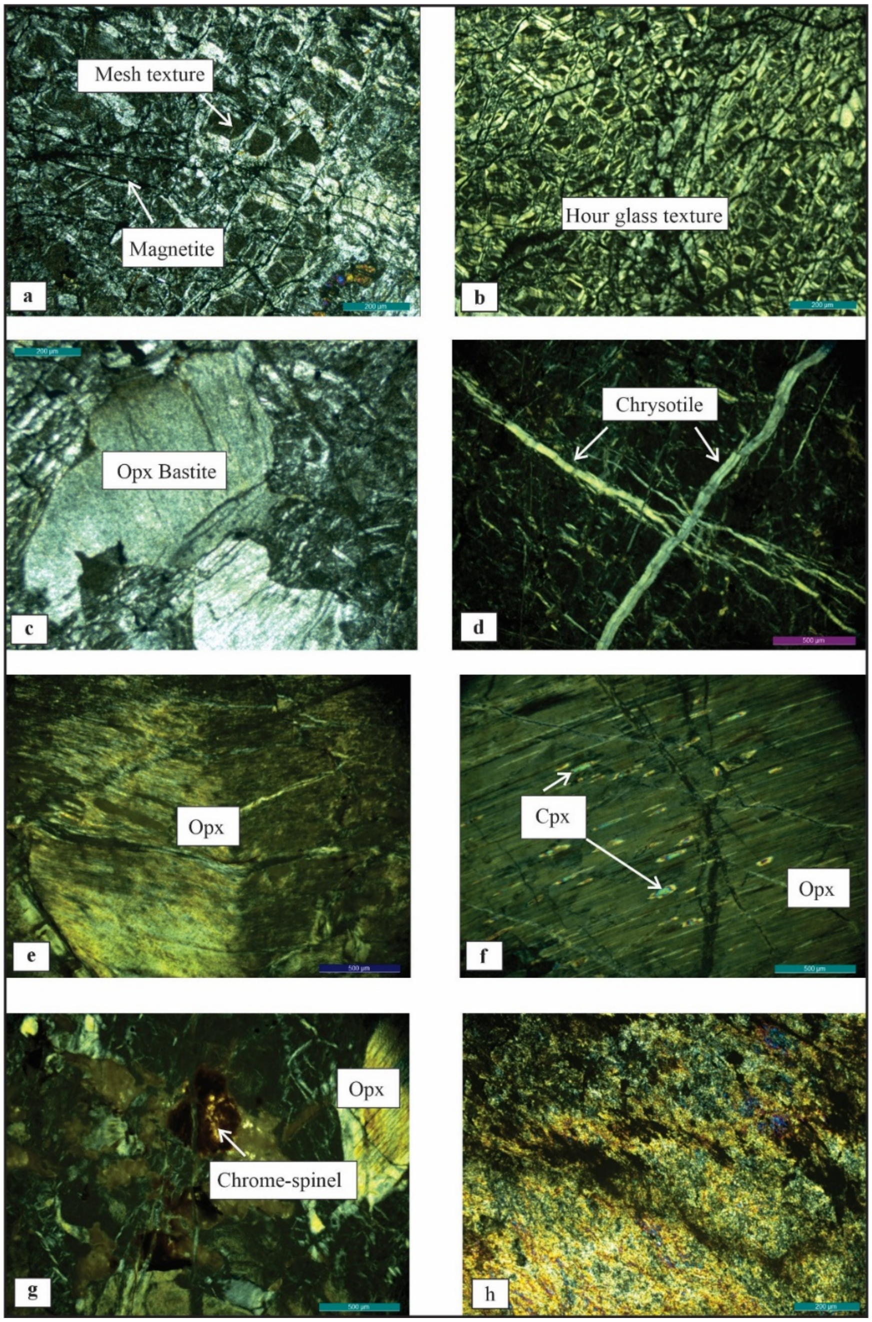


**Fig 2. Photomicrograph of serpentinite rocks under cross-polarized light (XPL) showing a) a mesh texture indicative of serpentinization within the peridotite and fine-grained magnetite filled along the boundary; b) hourglass textures of serpentine pseudomorphs replacing olivine; c) bastite pseudomorphs originating from orthopyroxene (Opx); d) Fibrous chrysotile veins observed in serpentinized ultramafic; e) Kink banding and undulatory extinction in Orthopyroxene; f) Orthopyroxene exsolve clinopyroxene (cpx) lamellae in serpentinite rocks; g) Chrome-Spinel occurs in between pyroxene and serpentinite; h) Serpentine mineral with alteration of Olivine and pyroxene**

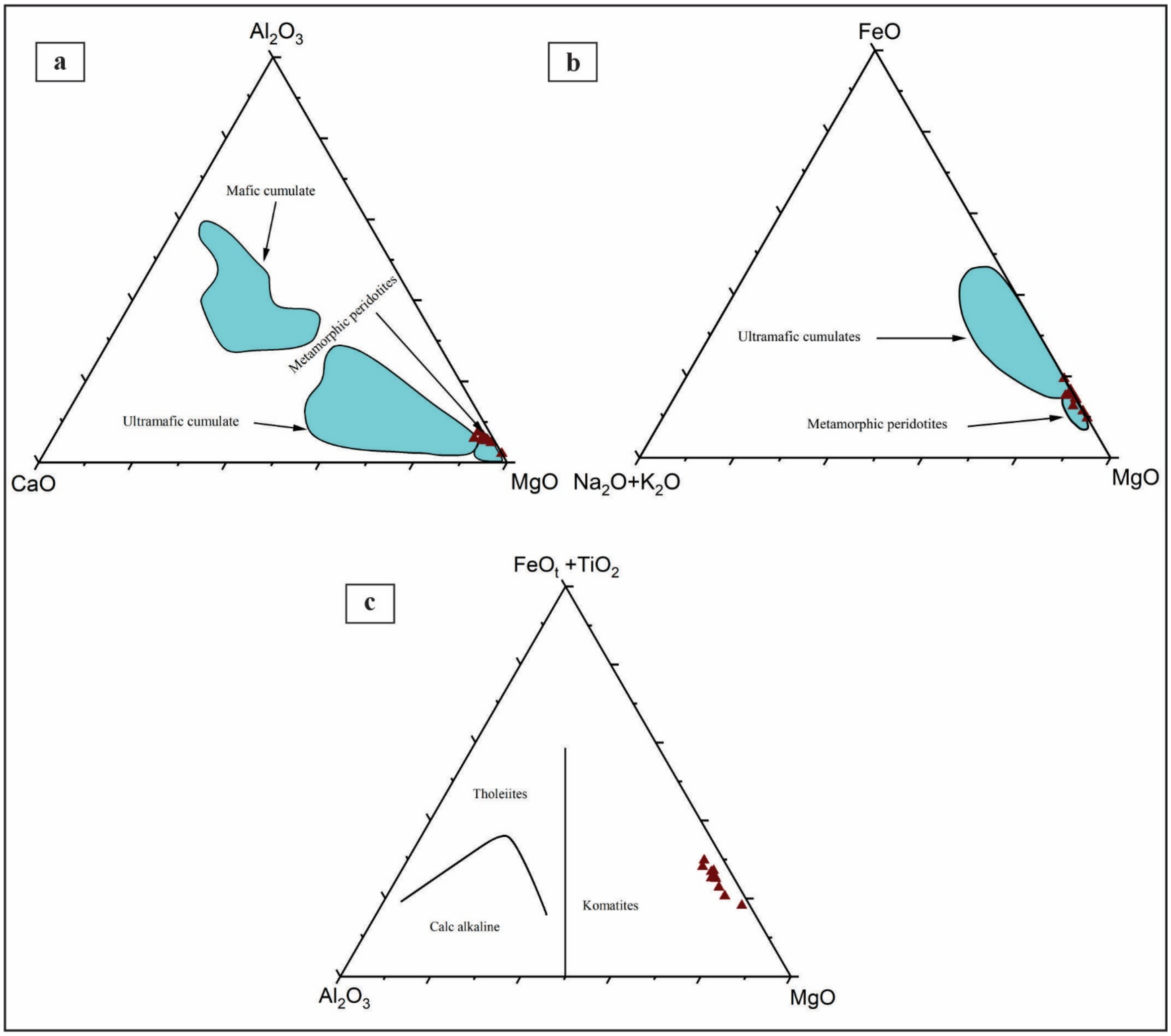


**Fig 3. Ternary plots of a) ACM ($Al_2O_3$–CaO–MgO); b) AFM [($Na_2O$ + $K_2O$)–FeO–MgO]; c) ($FeO_t$ +$TiO_2$)–$Al_2O_3$-MgO diagram, for the studied serpentinite rocks in MOC**

$Al_2O_3$, whereas $SiO_2$, $Fe_2O_3$, $Na_2O$, and $TiO_2$ are covariant with $Al_2O_3$. The samples also had low CaO contents ranging from 0.02 to 1.72 wt.%, and given CaO's high mobility, its depletion shows that clinopyroxene change is accompanied by Ca dissolution[(16,17)]. Furthermore, the examined serpentinites peridotites fall into the fields of abyssal mantle peridotites when major oxide compositions are compared to $Al_2O_3$ indicating a strong affinity with this mantle peridotite (Figure 4 ).

### 3.3 Trace and Rare earth elements:

The serpentinite rock samples are rich in transition metals such as Cr (628 to 3816 ppm), Ni (2264 to 4074 ppm), Co (31 to 126 ppm), V (6 to 90 ppm), and Cu (6 to 36 ppm), indicating their mantle origin. A trace element versus $Al_2O_3$ variation diagram (Figure 5)[(15)] shows that the majority of the samples correspond to mantle peridotites, including both abyssal and ophiolitic types. Elements such as Ni and Cr enrich the primitive mantle (PM) due to their compatibility with mantle minerals such as olivine and spinel. Furthermore, Yb versus $Al_2O_3$ trends show a positive correlation with $Al_2O_3$ in the tectonically emplaced abyssal peridotites.

The studied rocks show a significant depletion of rare earth elements (REE) and a low abundance of ΣREE. Chondrite-normalized REE (after McDonough and Sun 1995) patterns are slightly concave-up, displaying depletion in light REE (LREE), and are relatively flat in heavy REE (HREE), resembling a spoon (Figure 9**a**). The depletion in LREE $(La/Yb)_N$ = 0.021–4.253) is relatively more as compared to HREE $(Gd/Yb)_N$ = 0.429–1.002) and middle REE (MREE; $(Ce/Sm)_N$ = 0.218–4.050).

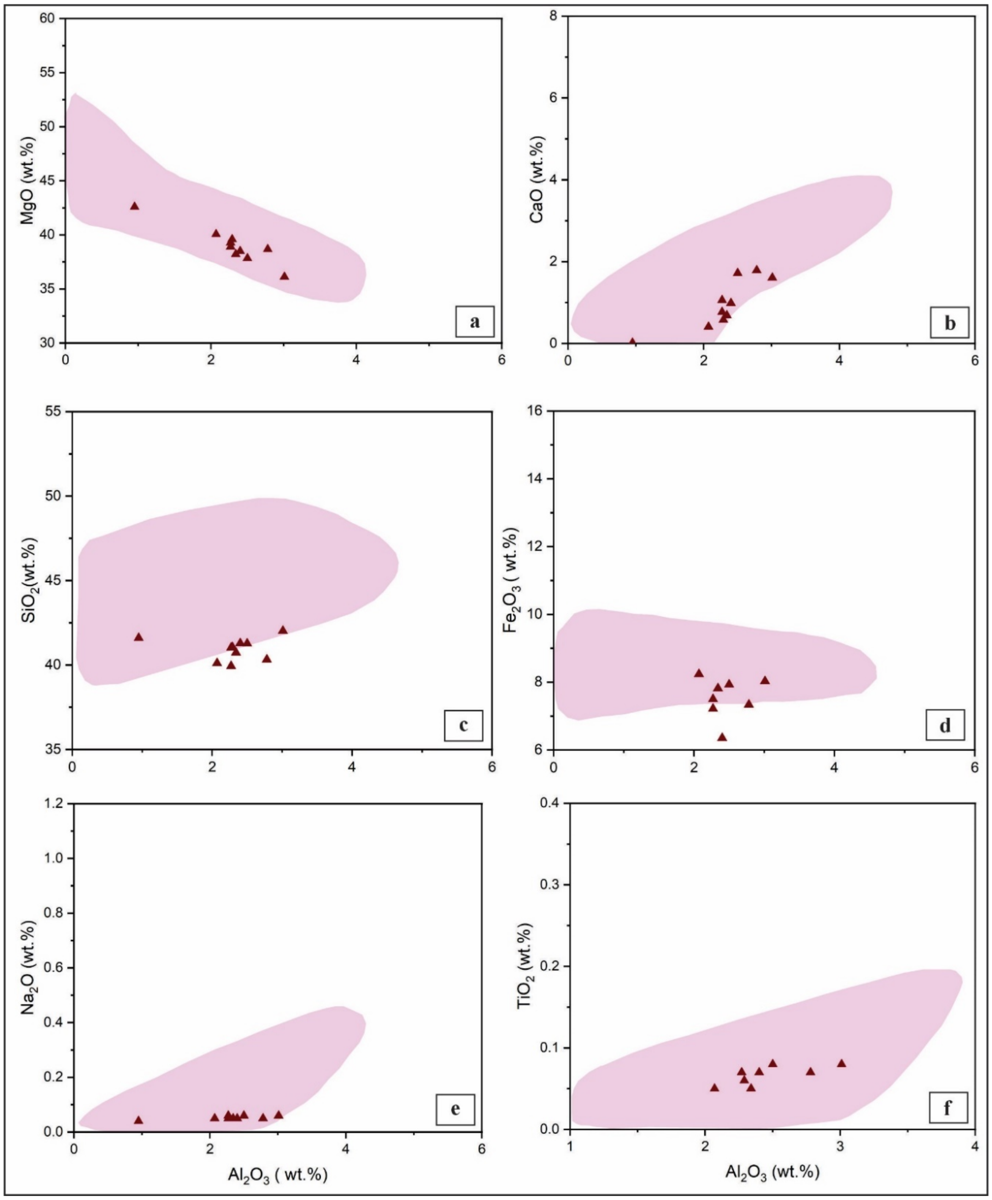


**Fig 4. Plots of selected major versus $Al_2O_3$ of the studied Serpentinite rocks a) MgO vs. $Al_2O_3$; b) CaO vs. $Al_2O$; c) $SiO_2$ vs. $Al_2O_3$ ;d) $Fe_2O_3$ vs. $Al_2O_3$; e) $Na_2O$ vs. $Al_2O_3$ and f) $TiO_2$ vs. $Al_2O_3$. The light purple fields are of orogenic, ophiolitic, and abyssal mantle peridotites**

Their REE patterns show positive Ce (Ce/Ce*: 0.348-3.552 with an average value of 1.33) and Eu (Eu/Eu*: 0.717–4.913 with an average of 1.27) anomalies. The observed positive Eu anomaly and the increase in LREE/HREE observed in the serpentinite can be attributed to the action of hydrothermal fluid. This is because serpentinites like their source rocks are depleted in REE. Serpentinite samples show negative anomalies for elements including Rb, Sr, Ce, and Eu, and positive anomalies for U, Y, and La on the multi-element diagrams normalized to the primitive mantle (after Sun and McDonough 1989). Their incompatible immobile elements ranging from Gd to Lu exhibit flat patterns, similar to those observed in abyssal peridotites[(15)] (Figure 9 **b**).

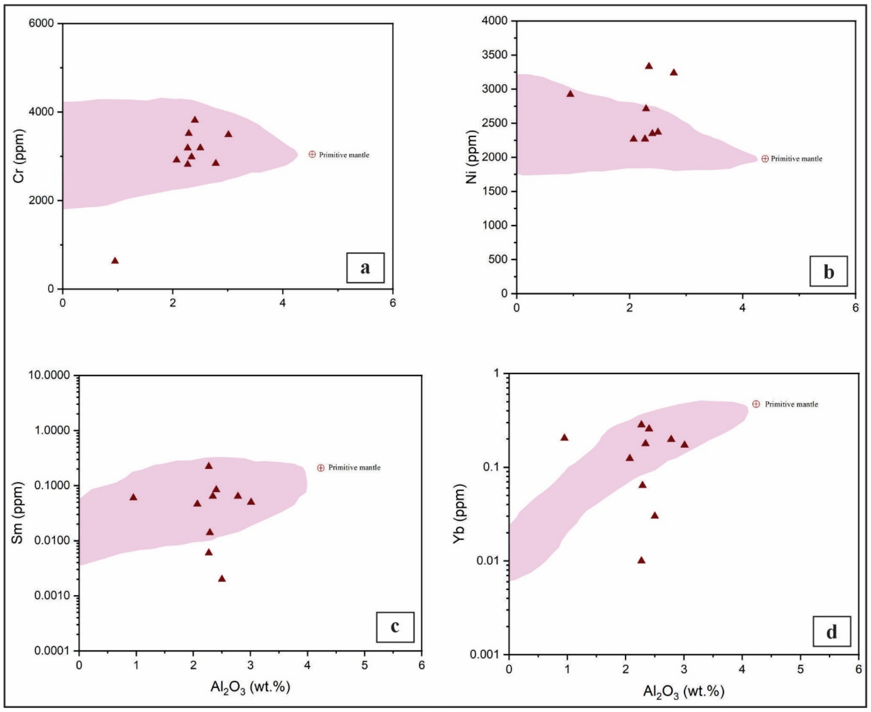


**Fig 5. Selected trace elements binary plots against $Al_2O_3$; a) Cr vs. $Al_2O_3$; b) Ni vs. $Al_2O_3$; d) Sm vs. $Al_2O_3$ and d) Yb vs $Al_2O_3$. Orogenic, ophiolitic, and abyssal mantle peridotites (light purple fields)**

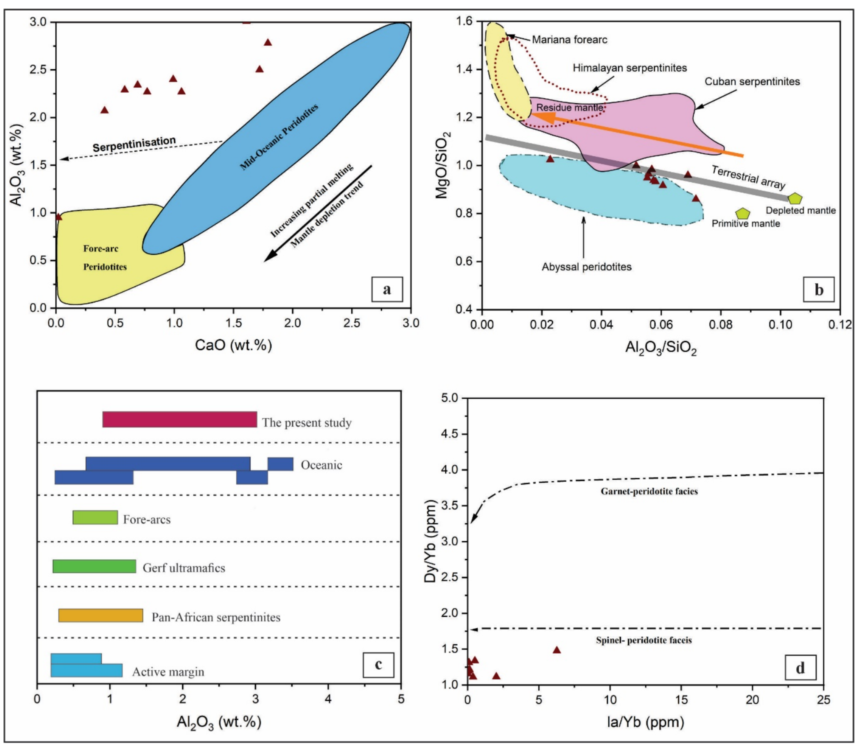


**Fig 6. a) Plots showing CaO vs. $Al_2O_3$ wt.% variation diagram of the studied serpentinite rocks. b) Whole-rock $MgO/SiO_2$ vs. $Al_2O_3/SiO_2$; c) Bulk-rock $Al_2O_3$ (wt. %) contents of serpentinites in MOC compared with those from other tectonic settings and the Pan-African serpentinites d) The Dy/Yb versus La/Yb plot for the serpentinite rocks indicates their formation at relatively shallow depths within the spinel-peridotite stability field**

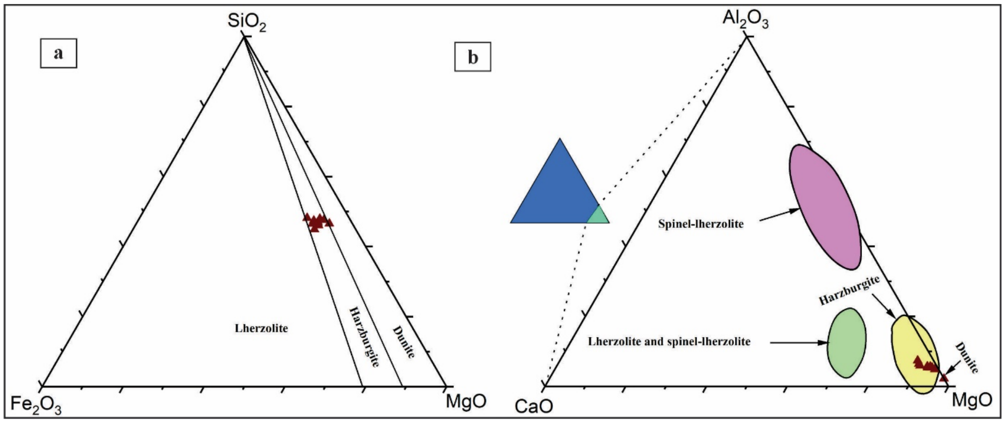


**Fig 7. a) SiO2-FeO*-MgO triangular diagram and (b) relationship between serpentinites and their protoliths in a MgO-$Al_2O_3$-CaO (wt%) ternary diagram of the studied serpentinite rocks**

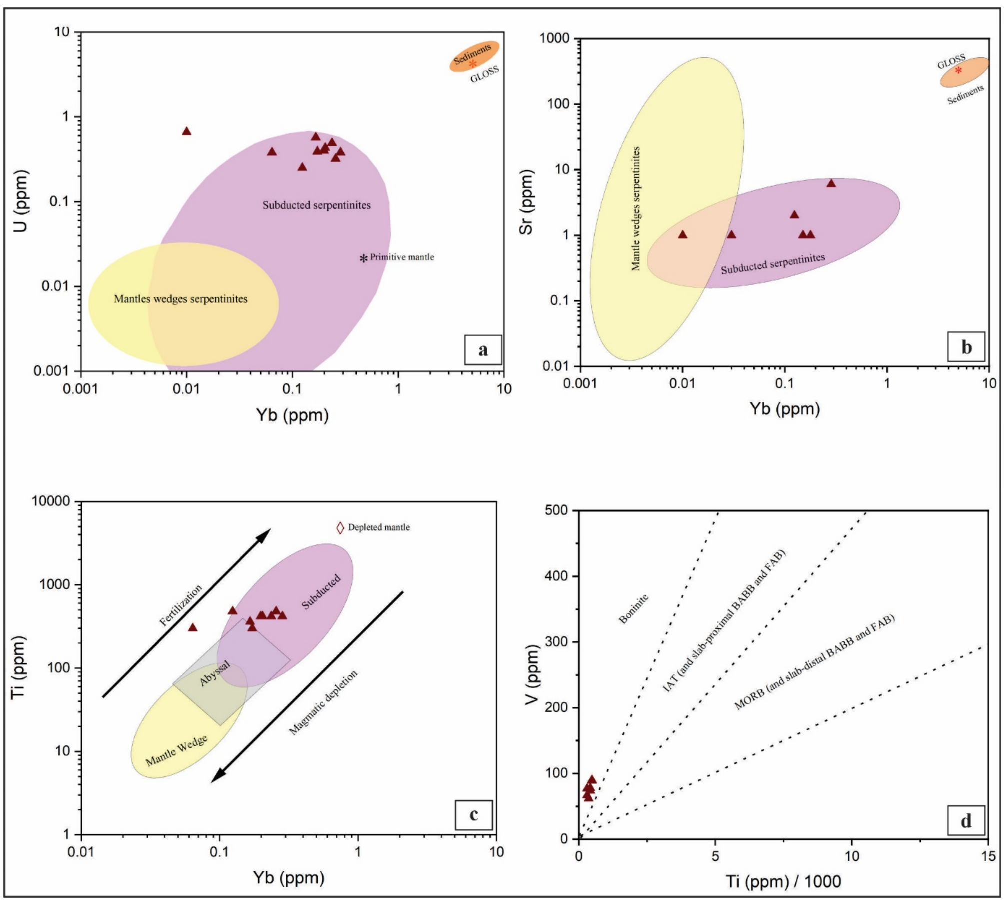


**Fig 8. Binary plots of a) U (ppm); b) Sr (ppm); c) Ti (ppm) against Yb (ppm) for the analyzed serpentinite rocks (the compositions of the primitive mantle, global subducting sediments (GLOSS), and sediments are included for comparison) and d) The Ti/1000 vs. V plot separates MORB, island arc tholeiite (IAT), and boninite magma types**

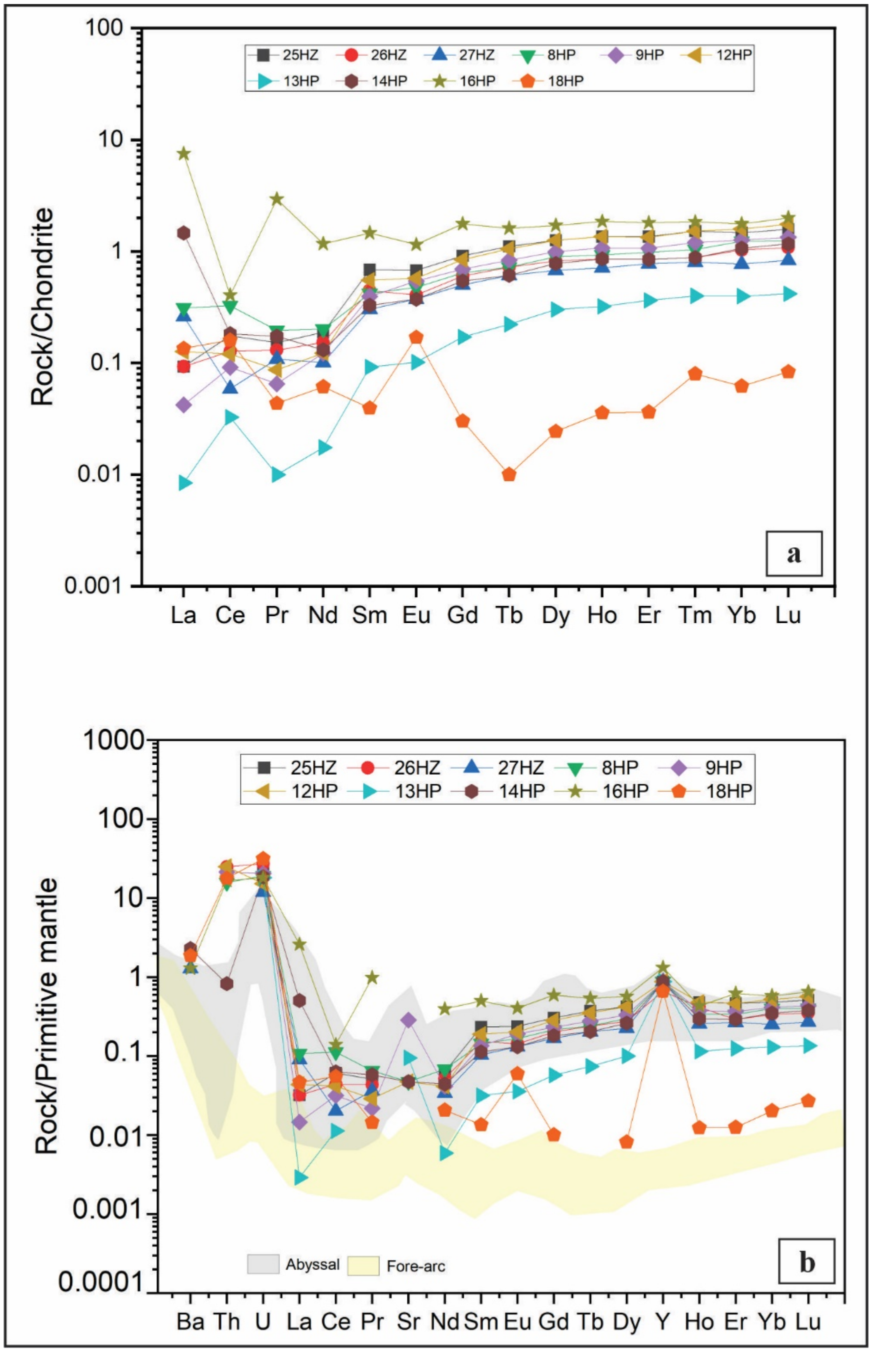


**Fig 9. a) Chondrite-normalized pattern of REE and b) Primitive mantle-normalized pattern of trace and REE. Field of abyssal peridotite (Grey) and field of fore-arc peridotites (Light yellow)**

# 4 Discussion

## 4.1 Nature and Origin of Serpentinites:

On the $Al_2O_3$ and CaO Binary diagram (Figure 6**a**)[16], the studied serpentinite rocks correspond to abyssal peridotite. On the $SiO_2$/MgO versus $Al_2O_3$/ $SiO_2$ diagram (Figure 6**b**)[16] the analyzed samples fall below the trend line for the 'mantle terrestrial array,' indicating a magmatic depletion (or enrichment) trend from primitive mantle compositions to highly depleted harzburgitic compositions. The majority of the samples fall within the abyssal peridotite fields. Residues exhibit higher Mg/Si and lower Al/Si ratios, whereas melts show the opposite with lower Mg/Si and higher Al/Si ratios. According to Niu (2004), abyssal serpentinites are characterized by low $Al_2O_3/SiO_2$ ratios (below 0.035) and $MgO/SiO_2$ ratios ranging from 0.8 and 1.2. In contrast, abyssal peridotites have $Al_2O_3/SiO_2$ ratios ranging from 0.01 to 0.07 and $MgO/SiO_2$ ratios from 0.75 to 1.05. According to Le Maître (1976), work suggests that average $MgO/SiO_2$ and $Al_2O_3/SiO_2$ ratios for specific rock types are 0.83 and 0.05 for harzburgite, 0.66 and 0.09 for lherzolite, and 0.99 and 0.04 for dunite, respectively.[17] Meanwhile, the serpentinite rocks in MOC have $MgO/SiO_2$ values between 0.86 and 1.02 with an average value of 0.95. The $Al_2O_3/SiO_2$ values ratio ranges between 0.05 and 0.07 with an average value of 0.04, likely resembling dunite. Also, on the plot of the $Fe_2O_3$-$SiO_2$-MgO and the CaO-$Al_2O_3$-MgO tri-plot, the studied samples plot in harzburgite with minor dunite (Figure 7**a** and **b**).[18] Therefore the studied serpentinites of MOC corresponds to a protolith of harzburgite and minor dunite. The serpentinite peridotites show a refractory nature, evidenced by high $MgO/SiO_2$ and high $Al_2O_3$ content (average = 2.29) which is relatively unaffected by serpentinization and therefore retains its original primary signature (Figure 6 **c**), similar to abyssal peridotites found at mid-ocean ridge settings[19]. Al/Si ratio ranges from 0.023 to 0.072 which indicates that these serpentinites are the refractory depleted mantle protolith and are lower than the primitive mantle (PM ~ 0.1) values but higher than highly depleted mantle residual harzburgites (~ 0.02). So, the depletion of Al in the analyzed samples represents refractory peridotite residues that have undergone partial melting, as Al is slightly incompatible with mantle minerals and is depleted during the processes. Thus, the studied serpentinites are derived from the alteration of harzburgite with a limited dunite protolith composition. This finding is bit contrast with the existing view that the MOC is primarily derived from lherzolitic protoliths.

The studied serpentinites rocks in the Dy/Yb versus La/Yb variation diagram correspond to Spinel-peridotite facies (Figure 6**d**). Dick and Bullen (1984) proposed a component of plagioclase peridotites, which make up ~30 vol% of abyssal peridotites on the seafloor, but plagioclase is absent in all the studied samples. The very low Ca (0.02–1.79 wt%) and Na (0.04–0.06 wt.%) contents in these samples give the clue that the original amount of plagioclase was low and was altered during serpentinization[16]. The results also showed depletion of major and trace elements in the rock compared to PM values. The depletion of rare earth elements (REE) and high-field-strength elements (HFSE) relative to PM has been observed in orogenic, abyssal, and ophiolite peridotites[15,16], indicating their origin as mantle melting residues.

## 4.2 Geo-tectonic environments:

Serpentinization occurs in various tectonic settings and is caused by the hydration of mafic or ultramafic rocks through interaction with fluids from different sources. Serpentinization of mantle rocks typically occurs during ocean-floor metamorphism at mid-ocean ridges and through dynamic metamorphism at subduction zones[20]. Previous workers[21,22] have demonstrated that the geochemistry of serpentinites is closely linked to their tectonic settings. Ocean-floor metamorphism results in the mobilization of trace elements like Rb and Sr, enrichment of Pb and Sb through carbonate precipitation, and U-enrichment due to hydrothermal alteration[16]. The titanium (Ti) contents of bulk rock are often used to determine the tectonic settings in which serpentinite is formed since Ti tends to remain stable and unchanged during serpentinization and is not significantly affected during melt-rock interactions. Specifically, mantle wedge serpentinites are characteristic of low bulk rock Ti content (2–50 ppm), while abyssal and subducted serpentinites have higher Ti concentrations, ranging from 10 to 130 ppm and above 50 ppm, respectively[23].

The studied serpentinite rocks show depletion in Rb and Sr and exhibit high LOI (average = 13.39 wt.%), indicating seafloor alteration. To assess the influence of subduction on SSZ lavas, various researchers plot mafic-ultramafic rocks on a Ti/1000 vs. variation diagram. Titanium (Ti) is highly incompatible and decreases with increasing partial melting, while vanadium (V) remains immobile and exhibits incompatible behavior under oxidizing conditions with the presence of fluids. The melting regime triggered by subduction fluids leads to depletion in Ti and enrichment in V. As a result, the ratio of Ti/V greater than 20 is typical of MORB, intermediate ratios (10-20) occur in island arc tholeiites, and lower ratios (<10) are commonly found in boninites. Thus, the serpentinized rocks have low Ti/V ratios ranging from 3.89 to 5.80, fitting within the boninite data range, suggesting formation at higher oxidizing conditions during subduction initiation (Figure 8**d**). The high Ti concentrations (averages = 400) are comparable to those of subducted serpentinites strongly support a subduction-related setting (Figure 8 **a, b**

**& c)** [24]. The high Cr contents and spinel protolith compositions indicate that the parent magmas were generated in a subduction environment, particularly in a Supra-Subduction Zone setting [25].

## 5 Conclusions

Comprehensive petrographic and geochemical analyses of serpentinite rocks in the MOC area have significantly expanded our understanding of their genesis and evolution. The sample shows mesh and hourglass textures pseudomorph after olivine and bastites after pyroxene. Higher Mg numbers (Mg# average 84.4), with high Cr (628 - 3816 ppm) and Ni (2264 to 4074 ppm) contents a komatiitic affinity of the studied samples originated from cumulate-derived mantle peridotite. The high LOI, low $Al_2O_3/SiO_2$ (0.02 to 0.07 wt.%), and high $MgO/SiO_2$ (0.86-1.02 wt.%) compared to the primitive mantle also suggest mantle residual harzburgite with limited dunite that had undergone varying degrees of serpentinization, which is similar to the oceanic abyssal peridotites. This study also reveals a unique transitional phase between abyssal and subduction-related serpentinite indicating a complex process occurring in supra-subduction environments. The high-Ti (> 50 ppm) content in the bulk rocks with boninitic mantle melt and spoon-shaped REE signatures indicates the subduction initiation. Therefore, the studied serpentinite rocks in MOC are derived in two distinct tectonic environments of abyssal or mid-oceanic ridge and subduction. More studies on the serpentinite rocks in MOC could offer important information about the evolution of supra-subduction environments together with the related magmatic & metamorphic processes. The results are also crucial for grasping the evolution of Earth's mantle and oceanic crust development through time, as well as the formation of economic mineral deposits related to ultramafic rocks. Further studies should focus on detailed mineralogy and P-T conditions of the ultramafic rocks and may give us a better understanding of the protolith's composition and evolution of these rocks.

### Acknowledgment

The first author (G.Lamzamuan) would like to thank the Council of Scientific and Industrial Research (CSIR), New Delhi, for providing financial assistance under the Junior Research Fellowship Scheme (File No. 09/864(0012)/2019-EMR-I) to carry out this work. The authors thank DST-SERB for funding the Leica microscope at the Department of Geology, Mizoram University, to carry out petrographic analysis.

## References

1) Verencar A, Saha A, Ganguly S, Manikyamba C. Tectono-magmatic evolution of Tethyan oceanic lithosphere in supra subduction zone fore arc regime: Geochemical fingerprints from crust-mantle sections of Naga Hills Ophiolite. *Geoscience Frontiers*. 2021;12(3):101096–101096. Available from: https://doi.org/10.1016/j.gsf.2020.10.003.
2) Singh AK, Chung S, Somerville ID. Petrogenesis of mantle peridotites in Neo-Tethyan ophiolites from the Eastern Himalaya and Indo-Myanmar Orogenic Belt in the geo-tectonic framework of Southeast Asia. *Geological Journal*. 2022;57(12):4886–919. Available from: https://doi.org/10.1002/gj.4629.
3) Dilek Y. Neotethyan Ophiolites and Their Geodynamic Evolution During the Mesozoic: A Global Overview. *Acta Geologica Sinica* . 2020;94(S1):76–77. Available from: https://doi.org/10.1111/1755-6724.14479.
4) Rogkala A, Petrounias P, Tsikouras B, Giannakopoulou PP, Hatzipanagiotou K. Mineralogical Evidence for Partial Melting and Melt-Rock Interaction Processes in the Mantle Peridotites of Edessa Ophiolite. *North Greece) Minerals*. 2019;9(2):120–120. Available from: https://doi.org/10.3390/min9020120.
5) Premi K, Sen AK, Singh AK, Lakhan N. Petrogenesis and tectonic environments for formation of peridotites and associated podiform chromite ore, southern part of Manipur Ophiolite Belt. *Neues Jahrb Für Mineral - Abh*. 2022;197(3):209–241. Available from: https://doi.org/10.1127/njma/2021/0255.
6) Khuman CM, Ibotombi S. Source characterisation of the residual lherzolite and harzburgite ultramafics of Manipur Ophiolite Belt in the Indo-Myanmar Hill ranges. *NE India Geological Journal*. 2022;57(12):5294–307. Available from: https://doi.org/10.1002/gj.4493.
7) Chaubey M, Singh AK, Singh BP, Imtisunep S, Dutt A, Satyanarayanan M. Refertilization of depleted mantle peridotite in the Nagaland-Manipur ophiolite, north-east India: Constraints from PGE , mineral, and whole-rock geochemistry. *Geological Journal*. 2022;57(12):5265–83. Available from: https://doi.org/10.1002/gj.4411.
8) Kingson O, Liu Y, Bhutani R, Widdowson M. Relicts of Neo-Tethyan mantle wedge in the Indo-Burma Range, India: Record of carbonate metasomatism and Neo-Tethyan mantle evolution. *Results in Earth Sciences*. 2023;100001. Available from: https://doi.org/10.1016/j.rines.2023.100001.
9) Khogenkumar S, Singh AK, Kumar S, Lakhan N, Chaubey M, Imtisunep S. Subduction versus non-subduction origin of the Nagaland-Manipur Ophiolites along the Indo-Myanmar Orogenic Belt, northeast India: Fact and fallacy. *Geological Journal*. 2021;56(4):1773–94. Available from: https://doi.org/10.1002/gj.4030.
10) Imtisunep S, Singh AK, Bikramaditya R, Khogenkumar S, Chaubey M, Kumar N. Evidence of intraplate magmatism and subduction magmatism during the formation of Nagaland-Manipur Ophiolites. *Geological Journal*. 2022;57(2):782–800. Available from: https://doi.org/10.1002/gj.4378.
11) Khin K, Moe A, Aung KP. Tectono-structural framework of the Indo-Myanmar Ranges: Implications for the structural development on the geology of the Rakhine Coastal Region. *Myanmar Geosystems and Geoenvironment*. 2022;1(3):100079–100079. Available from: https://doi.org/10.1016/j.geogeo.2022.100079.
12) Ao A, Bhowmik SK, Upadhyay D. P-T-melt/fluid evolution of abyssal mantle peridotites from the Nagaland Ophiolite Complex, NE India: Geodynamic significance. *Lithos*. 2020. Available from: https://doi.org/10.1016/j.lithos.2019.105344.
13) Sahu A, Vishwakarma N, Santosh M, Singh Y, Hari KR. Petrogenesis of ultramafic rocks with abyssal peridotite affinity from the Central Bundelkhand Craton. *India Geosystems and Geoenvironment*. 2024;3(1):100221–100221. Available from: :https://doi.org/10.1016/j.geogeo.2023.100221.

14) Wang M, Li PX, R, Li PL, Liu Z, C. Timing of Transition from Proto- to Paleo-Tethys: Evidence from the Early Devonian Bimodal Volcanics in the North Qaidam Tectonic Belt. *Northern Tibetan Plateau Minerals*. 2023;13(4). Available from: https://doi.org/10.3390/min13040532.
15) Bhat IM, Ahmad T, Rao S, V D. Origin and evolution of Suru Valley ophiolite peridotite slice along Indus suture zone, Ladakh Himalaya, India: Implications on melt-rock interaction in a subduction-zone environment. *Geochemistry*. 2019;79(1):78–93. Available from: https://doi.org/10.1016/j.chemer.2018.10.003.
16) Tsoungui NEP, Ganno S, Njiosseu TE, Mbongue JLN, Woguia KB, Tamehe SL, et al. Geochemical constraints on the origin and tectonic setting of the serpentinized peridotites from the Paleoproterozoic Nyong series, Eseka area, SW Cameroon. *Acta Geochimica*. 2020;39(3):404–426. Available from: https://doi.org/10.1007/s11631-019-00368-4.
17) Zhou D, Cao S, Liu J, Li X, Dong Y, Neubauer F. Carbonation and serpentinization of diopsidite in the Altun Mountains, NW China. *Scientific Reports*. 2022;12(1):1–15. Available from: https://doi.org/10.1038/s41598-022-25612-5.
18) Abdel-Karim AM, Azer MK, El-Shafei SA. Petrology and Geochemistry of Some Ophiolitic Metaperidotites from the Eastern Desert of Egypt: Insights into Geodynamic Evolution and Metasomatic Processes. *Acta Geologica Sinica - Engl Ed*. 2021;95(4):1139–1157. Available from: https://doi.org/10.1111/1755-6724.14688.
19) Sedki T, Ali S, Mohamed HA. Geochemistry dataset of the Sol Hamed Neoproterozoic ophiolitic serpentinites, southern Eastern Desert. *Egypt Data Brief*. 2019;25:104393–104393. Available from: https://doi.org/10.1016/j.dib.2019.104393.
20) Raia NH, Whitney DL, Teyssier C, Lesimple S. Serpentinites of Different Tectonic Origin in an Exhumed Subduction Complex. In: Geochemistry, Geophysics;vol. 23. 2022. Available from: :https://doi.org/10.1029/2022GC010395.
21) Wu K, Ding X, Ling MX, Sun W, Zhang LP, Hu YB, et al. Origins of two types of serpentinites from the Qinling orogenic belt, central China and associated fluid/melt-rock interactions. *Lithos*. 2018;302-303:50–64. Available from: https://dx.doi.org/10.1016/j.lithos.2017.12.019.
22) Gilio M, Scambelluri M, Agostini S, Godard M, Peters D, Pettke T. Petrology and Geochemistry of Serpentinites Associated with the Ultra-High Pressure Lago di Cignana Unit (Italian Western Alps). *Journal of Petrology*. 2019;60(6):1229–1262. Available from: https://dx.doi.org/10.1093/petrology/egz030.
23) Yin ZZ, Chen RX, Zheng YF, Gong B, Zha XP, Xia X. Serpentinization and Deserpentinization of the Mantle Wedge at a Convergent Plate Margin: Evidence of Orogenic Peridotites from a Composite Oceanic–Continental Subduction Zone. *Journal of Petrology*. 2023;64(3). Available from: https://dx.doi.org/10.1093/petrology/egad015.
24) Jalil R, Alard O, Schaefer B, Ali L, Sajid M, Khedr MZ, et al. Geochemistry of Waziristan Ophiolite Complex, Pakistan: Implications for Petrogenesis and Tectonic Setting. *Minerals*. 2023;13(3):311–311. Available from: https://dx.doi.org/10.3390/min13030311.
25) Abuamarah BA, Asimow PD, Azer MK, Ghrefat H. Suprasubduction-zone origin of the podiform chromitites of the Bir Tuluhah ophiolite, Saudi Arabia, during Neoproterozoic assembly of the Arabian Shield. *Lithos*. 2020;360-361:105439–105439. Available from: https://dx.doi.org/10.1016/j.lithos.2020.105439.